crystals

MDPI

Article

Noise-Induced Defects in Honeycomb Lattice Structure: A Phase-Field Crystal Study

Vladimir Ankudinov [1,2,†] and **Peter K. Galenko** [3,*,†]

[1] Institute of Mathematics, Information Technologies and Physics, Udmurt State University, 426034 Izhevsk, Russia; vladimir@ankudinov.org
[2] Theoretical Department, Vereshchagin Institute for High Pressure Physics, Russian Academy of Sciences, 108840 Troitsk, Moscow, Russia
[3] Physikalisch-Astronomische Fakultät, Friedrich-Schiller-Universität, 07743 Jena, Germany
* Correspondence: peter.galenko@uni-jena.de
† These authors contributed equally to this work.

Abstract: One of the classes of the kinetic phase-field model in the form of the two-mode hyperbolic phase-field crystal model (modified PFC model) is used for the study of the noise effect of the crystalline structure. Special attention is paid to the origin of the defect's microstructure in the crystalline honeycomb lattice due to induced colored noise. It shows that the noise–time correlation coefficient τ_ζ, comparable to the diffusion time, enhances the grain boundary mobilities. Instead, a small spatial correlation coefficient, λ_ζ, close to the first lattice parameter of the honeycomb crystal, stabilizes the structure. The finite non-zero value of the relaxation time τ for the atomic flux significantly slows the local relaxation of the fluctuated field and leads to the grains' fragmentation and formation of the disordered phases. The obtained results are applicable to the hexagonal atomic structures and, in particular, to honeycomb crystals, such as boron nitride, in which the lattice defects might be simulated through the induced colored noise.

Keywords: crystal lattice; atomic structure; colored noise; phase-field crystal; model

Citation: Ankudinov, V.; Galenko, P.K. Noise-Induced Defects in Honeycomb Lattice Structure: A Phase-Field Crystal Study. *Crystals* **2024**, *14*, 38. https://doi.org/10.3390/cryst14010038

Academic Editor: George D. Verros

Received: 23 November 2023
Revised: 8 December 2023
Accepted: 15 December 2023
Published: 27 December 2023

1. Introduction

Material properties, such as plasticity, (micro)hardness, and thermal and electrical conductivity are directly determined by the perfect crystalline structure and, accordingly, the presence of defects in the crystals. Therefore, in the mid-past century, particular attention was paid to the occurrence of crystal lattice defects due to their influence on the properties of the material [1].

Generally, one can distinguish among various types of crystal lattice defects, such as pointed defects (vacancies, vesicles), spatially extended violations of lattice ideality (dislocations and disclinations), grain boundaries with imperfections, and cracks. All classes of defects can arise during the process of natural relaxation of a sample, for example, when it is cooled from a high-temperature region to a given temperature with thermal shrinkage, as well as with removing the pressure and loading.

One of the modern and necessary methods for solving problems seems to be to find ways to strengthen materials operating under heavy loads and under exposure to aggressive environments. The latter is due to chemical or radiation effects on the surface of the sample with its penetration into the volume of the material. Distortion of the lattice, including disruption of the continuity of the crystallite with its subsequent destruction, can be a consequence of the radiation penetration of active neutrons onto the working surface and into the volume of the chemical and atomic reactors. Because these defects originate under irradiative interaction, special investigations are carried out on different spatial lengths and different temporal scales [2].

Recently, honeycomb crystals have been studied using the phase-field crystal model (PFC model) and its modifications. A modification of PFC for two-dimensional heterostructures was presented in work [3]. The model concludes by extending the binary single-mode PFC with a Gaussian smoothing kernel in correlation terms, implementing an idea closely related to the Structural PFC (XPFC) that includes excess terms for free energies. A study of the transitions between quadratic and hexagonal lattices in two-mode PFC under elevated pressure was performed in Ref. [4]. A number of ideas, including the detailed study and extended description of grain boundary migration, solid–solid transitions, and defects' motion, were published in work [5]. These works were devoted to studies of squared/cubic lattices; therefore, the focus of the present study is the evolution of honeycomb crystals under the influence of noise. For this study, the two-mode phase-field crystal equation is chosen. Efficient and energy-stable numerical schemes for the two-mode phase-field crystal equation have been suggested in Ref. [6]. These schemes can be compared with the numerical scheme performed in the direct space of the present work. In particular, the present work extends the investigation of the growth and formation of two-dimensional hexagonal lattices based on the one- and two-mode binary modified PFC model (MPFC-model) [7–9]. For modeling of the initially ideal honeycomb lattice, we use two-triangular reciprocal lattices, for details, see Ref. [8].

The present work is also devoted to examining changes in the crystal lattice under the influence of external factors, one of which may be the exposure of the material to irradiation. Using a theoretical approach, this irradiation may be modeled by correlated colored noise [10,11] The colored noise is applied to the honeycomb to study the defects in a crystalline lattice induced by radiation. We model distortion as well as the originating boundaries between grains that appear as a result of noise-induced action on the initial ideal honeycomb lattice of a two-dimensional crystal. To investigate noise-induced lattice defects, we use the phase-field crystal model with colored noise formally described in the work [12]. Because the parameters of the colored noise are responsible for defects origination, we tried to quantify the values of space–time correlation factors that influence the imperfections appearing in the honeycomb crystalline lattice.

2. Two-Mode PFC Model with Noise

The kinetic phase field takes into account both the slow and fast regimes of phase transitions occurring under relatively small and large driving forces, respectively [13]. One of the versions of the kinetic phase-field model is known as the hyperbolic version of phase-field models [14,15], which, in the context of of PFC models, has been distributed as the PFC model with memory [16] or the modified phase-field crystal model (MPFC model) [17,18]. In its initial formulation, the MPFC model incorporates both fast elastic relaxation and slower mass diffusion [19,20]. Similar models may appear in other branches of science. For example, the consideration of particle diffusion in molecular liquids may yield such a model coming from the dynamical density functional theory [21].

In the present work, we state the MPFC model for the description of the relaxation of the average atomic concentration field n and the relaxation of the atomic density flux by the partial differential equation (PDE) of the hyperbolic type:

$$\tau \frac{\partial^2 n}{\partial t^2} + \frac{\partial n}{\partial t} = M\nabla \cdot \left[\nabla \frac{\delta F}{\delta n} + A\vec{\zeta} \right], \tag{1}$$

where τ is the relaxation time of the atomic density flux, M is the mobility that sets the time scale for the relaxation of the conserved order parameter n, and $\delta F/\delta n = \mu(n)$ represents the functional derivative in a form of the chemical potential as the driving force. The PDE (1) is a consequence of the Lyapunov requirement that the free energy of the entire domain is not increased during its relaxation to global equilibrium [22,23].

The last term on the right-hand side of PDE (1) appears as the noise ζ with the amplitude A. The spatial and temporal noise correlations are given by the reaction–diffusion equation [24]:

$$\tau_\zeta \frac{\partial \vec{\zeta}}{\partial t} = -\left(1 - \lambda_\zeta^2 \nabla^2\right)\vec{\zeta} + \vec{\xi}(\vec{r}, t), \tag{2}$$

where $\xi(\vec{r}, t)$ is a pure, white, delta-correlated noise with the parameters $\langle \xi(\vec{r}, t) \rangle = 0$, $\langle \xi(\vec{r}, t)\xi(\vec{r}', t') \rangle = 2\delta(\vec{r} - \vec{r}')\delta(t - t')$. The solution of Equation (2) gives the parameters of the colored noise source ζ [24]:

$$\vec{C}_r(\vec{r} - \vec{r}') = (\sqrt{2\pi}\lambda_\zeta)^{-d} \exp\left[-\frac{|\vec{r} - \vec{r}'|^2}{2\lambda_\zeta^2}\right]; \qquad C_t(t - t') = \tau_\zeta^{-1} \exp\left[-\frac{|t - t'|}{\tau_\zeta}\right]. \tag{3}$$

A special investigation of the system of Equations (1)–(3) was performed in [25] under the description of spinodal decomposition.

The dimensional case of the free energy functional F can be obtained using the density functional theory with the fitting of the coefficients for accurate accounting of the elastic coefficients [26,27]. Following previous works [15,23], the dimensionless equilibrium the free energy contribution F_{eq} as a function of n can be written as

$$F_{eq}[n] = \int \left[\frac{n}{2}\mathcal{L}_R n - \frac{a}{3}n^3 + \frac{v}{4}n^4\right] d\vec{r}, \tag{4}$$

In particular, the phenomenological parameters a and v in Equation (4) can be fitted to various physical properties as discussed in the literature [26–29]. The operator $\mathcal{L}_R$ in the single-mode approximation $R = 1$ is given by

$$\mathcal{L}_1 \equiv \Delta B_0 + B_0^x(\nabla^2 + q_0^2)^2. \tag{5}$$

The form of the PFC free energy Equation (4) in the single-mode approximation Equation (5) is strongly related to the energy of the periodic phase in the weak crystallization theory of liquid crystals [30,31].

For FCC or honeycomb crystal lattices (as well as for more complicated structures), the operator $\mathcal{L}_R$ can be derived via the two-mode approximation $R = 2$, as in [28,32,33]:

$$\mathcal{L}_2 \equiv \Delta B_0 + B_0^x(r_0 + (\nabla^2 + q_0^2)^2)(r_1 + (\nabla^2 + q_1^2)^2). \tag{6}$$

Here, the coefficients r_0, r_1, q_0, and q_1 allow one to fit the peak of the pair correlation function to the experimental one or to that obtained via molecular dynamics [34]. Using operator (6), the two-mode approximation of the MPFC equation (1) allows one to predict the results of atomistic simulation on front kinetics essentially better than its single-mode representation of the free energy through operator (5) in the whole range of driving forces accessible in the computational experiments; see Ref. [34]. The coefficients q_0 and q_1 correspond to the equilibrium lattice parameters of the first and second coordination spheres, respectively. r_0 and r_1 are stabilizing coefficients [33–35]. The gradient expansion of the correlation function introduces melting and crystallization in two-dimensional and three-dimensional periodic systems [36,37].

Operators (5) and (6) include $\Delta B_0 = B_0^\ell - B_0^x$ as the driving force defined by the difference between the dimensionless liquid-state bulk modulus B_0^ℓ and the elastic modulus B_0^x. ΔB_0 is a control parameter similar to the quenching depth. To determine the scales for the temperatures during the transition, one can use the driving force in the PFC-type model as the dimensionless quenching depth below the melting temperature [15,34]. The dimensionless quenching depth is $\varepsilon = \Delta T / T_m$, where $\Delta T = T_m - T$ is the undercooling and T_m is the melting temperature. As a result, one can define undercooling as

$$\Delta T = T_m(\Delta B_0 - \Delta B_0^*)/\Delta B_0^*; \quad \text{and} \quad \varepsilon = (\Delta B_0 - \Delta B_0^*)/\Delta B_0^*. \tag{7}$$

Here, ΔB_0 is a specific driving force adopted for the considered structure, and $\Delta B_0^* = 2a^2/(9v)$ is the driving force corresponding to the melting temperature [34]. The coefficients a and v present the generalized form of the free energy and the governing equation of motion independently of the particular values (see Equation (4) and Ref. [34]).

Even in the case of delta-like white noise, one can describe the nucleation of a new phase and model the dynamics of phase transformations [38] similarly to the weak crystallization given by the Landau–Brazovskii theory [30,31]. In the general case of colored noise, introducing the fluctuations (2) and (3) into Equation (1) leads to nontrivial pathways of transformation [12].

3. Details of the Numerical Simulation

The numerical solution of Equation (1) with the two-mode operator (6) has been performed in direct space using the finite element method (FEM) in COMSOL Multiphysics [39]. The numeric discrete approximation has been made using triangular second-order Lagrangian finite elements. Using the direct solver PARDISO of COMSOL Multiphysics software, the solutions have been performed by a dual-processor server-based AMD EPYC 7302 machine.

3.1. The Governing System of Equations for Numerical Simulation

To reduce the spatial derivative order of Equation (1), the new variables P_2, P_4, P_6, and P_8 were introduced according to Refs. [23,40]:

$$\begin{cases} \tau\dfrac{\partial^2 n}{\partial t^2} + \dfrac{\partial n}{\partial t} = M\nabla\cdot\left[\nabla\mu + A\vec{\zeta}\right], \\ \dfrac{\delta F}{\delta n} = \mu = \left(\Delta B_0 + B_0^x Q_1\right)n - an^2 + vn^3 \\ \qquad\qquad + B_0^x\nabla^2(2Q_2 n + Q_3 P_2 + 2Q_4 P_4 + P_6), \\ P_2 = \nabla^2 n, \\ P_4 = \nabla^2 P_2, \\ P_6 = \nabla^2 P_4, \\ \tau_\zeta\dfrac{\partial\vec{\zeta}}{\partial t} = -\left(1 - \lambda_\zeta^2\nabla^2\right)\vec{\zeta} + \vec{\xi}. \end{cases} \tag{8}$$

Here, the variable vector $\vec{\xi}$ is an uncorrelated and normally distributed ($\sigma = 1$) random variable that produces the colored noise variable vector $\vec{\zeta}$ via Equations (2) and (3). The noise amplitude A was initiated at $t = 300$, so the initial hexagonal crystal was first relaxed, and then the noise source was applied. The noise was generated using a pseudorandom source with the same seed for all parameters to control the regions of grain formation.

The constants Q_1–Q_4 include the parameters q_0, q_1, r_0, and r_1 as follows:

$$\begin{aligned} &Q_1 = q_0^4 q_1^4 + q_0^4 r_1 + q_1^4 r_0 + r_0 r_1, \;\; Q_2 = q_0^2(q_1^4 + q_0^2 q_1^2 + r_1) + q_1^2 r_0, \\ &Q_3 = q_0^4 + 4q_0^2 q_1^2 + q_1^4 + r_0 + r_1, \;\; Q_4 = q_0^2 + q_1^2. \end{aligned} \tag{9}$$

The second-order time derivative was calculated by the fifth-order backwards-differential formula. To obtain the structure factor $S(k)$, we use the similar normalization coefficient equal to 2×10^{-3}. The Fourier transform $\mathfrak{F}(n)$ of the atomic density field n was performed using the COMSOL integration operator of the fourth order.

3.2. Honeycomb Lattice and Nonequilibrium Contribution to the Free Energy

The numerical solution of Equation (8) in a two-dimensional domain was initiated with the periodical crystal obtained by the analytical representation of the hexagonal honeycomb crystal [8]:

$$n_{hon} = n_0 + \eta_A \left(\cos(qx) + \cos\left(\frac{qx}{2} + \sqrt{3}\frac{qy}{2} \right) + \cos\left(\frac{qx}{2} - \sqrt{3}\frac{qy}{2} \right) \right) - \eta_B \frac{3}{2} \left(\cos\left(qx + \frac{qy}{\sqrt{3}} \right) + \cos\left(qx - \frac{qy}{\sqrt{3}} \right) + \cos\left(2\frac{qy}{\sqrt{3}} \right) \right), \quad (10)$$

where n_0 is the average dimensionless honeycomb density; η_A and η_B are the density wave amplitudes for the first and second sublattices, respectively; and $q = 1$. The numerical parameters used in the calculations are presented in Table 1.

Table 1. The computational parameters of the two-mode MPFC model.

Property	Value	Property	Value
M (-)	1	τ (-)	1×10^{-2}
a (-)	0	ΔB_0 (-)	-0.95
v (-)	1	B_0^x (-)	1
r_0 (-)	-0.2	q_0 (-)	1
r_1 (-)	0.1	q_1 (-)	1
n_0 (-)	-0.55		

The free energy calculation $F[n, \vec{J}] = F_{eq}[n] + F_{neq}[\vec{J}]$ with the local equilibrium (4) and the nonequilibrium contribution $F_{neq}[\vec{J}]$ requires the computation of the flux variable $\vec{J}$ at each numerical time step [12,23]:

$$\tau \frac{\partial \vec{J}}{\partial t} = -\vec{J} - \vec{\nabla}\mu + A\vec{\zeta}(\vec{r}, t); \quad \text{and} \quad F_{neq}[\vec{J}] = \frac{\tau}{2} \int_\Omega \vec{J} \cdot \vec{J} d\Omega, \quad \tau > 0. \quad (11)$$

As a result, Equation (11) was solved with Equation (8) by time integration with a fixed time step $\delta t = 10^{-3}$. The two-dimensional computational domain consists of 200×200 dimensionless units with a mesh size ℓ of up to 1.1 along the side. The convergence on each time step was controlled with a relative tolerance of $\delta E = 10^{-7}$.

3.3. Calculation of the Noise-Induced Defects

In the present simulation, calculations of defects are performed from the initially ideal honeycomb lattice, which begins to change due to imposed noise of different intensities, i.e., different temporal and spatial dispersion. More specifically, in the case of a correlated noise source, the initial stable honeycomb crystal is exposed to noise sources with different amplitudes A (temperature) and spatial and temporal characteristics λ_ζ and τ_ζ. To investigate the effect of noise on defect formation, we performed the following simulations:

- Uncorrelated white noise, i.e., when the last equation of Equation (8) is terminated and one has $\vec{\zeta} = \vec{\xi}$;
- Spatio-temporal correlated noise, for a full system of Equation (8);
- Separate simulations with or without relaxation of the atomic density flux, i.e., with $\tau \neq 0$ or $\tau = 0$, respectively, in Equation (8).

The simulations provide results for different free energy profiles and relaxed atomic density n distributions. All of the simulations were performed in the region of the parameters (see Table 1) corresponding to the stable honeycomb phase [8,9]. As a qualitative outcome of the simulations, one can distinguish the following types of honeycomb lattice changes obtained due to the imposed noise of various types of dispersion:

- Distortions and rotations in the crystal lattice;
- The appearance of grains and boundaries between them.

4. Results and Discussion

4.1. Initial Distribution

The initial stable honeycomb crystal was constructed using Equation (10). The corresponding atomic density n and its Fourier distribution $\mathfrak{F}(n)$ are presented in Figure 1a,b. After the initial relaxation, this structure was saved as the honeycomb crystal in the absence of noise (Figure 1c,d) when the noise amplitude coefficient was set to $A = 0$ in Equation (8). The resulting slightly distorted honeycomb crystal with no defects is represented by the blurred reflections in the Fourier image (see the blurred points in Figure 1d and the relatively sharp points shown in Figure 1b). The appearance of the blurred points and peaks (see Figure 2) during the relaxation without noise, occurs due to the periodic boundary conditions of the square domain, which act as a distortion actuator when the layering of an even number of lattice parameters is impossible along the domain. Such a problem occurs in many cases during the two-mode PFC simulations [9,41] due to the presence of two lattice parameters, however, such a problem is absent in the case of the single-mode PFC approximation in which only the lattice parameter is accepted for calculations.

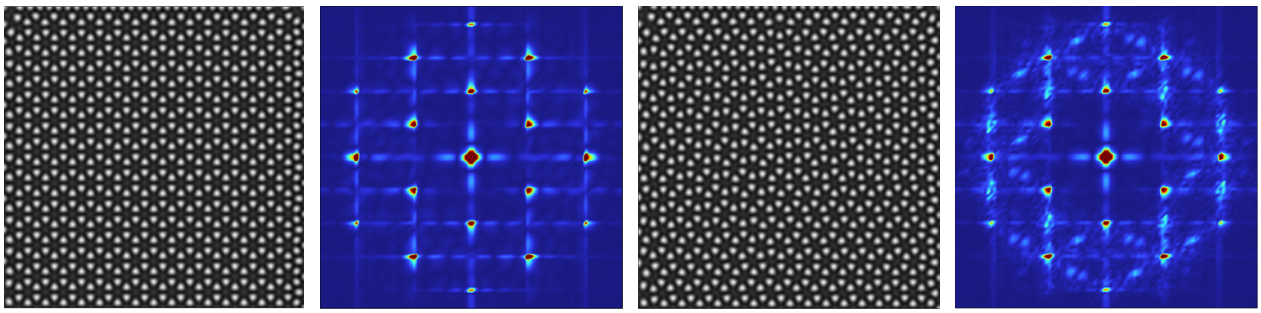

Figure 1. Snapshots of the density field n (**a**,**c**), and corresponding Fourier transforms $\mathfrak{F}(n)$ (**b**,**d**). (**a**,**b**) Initial distribution of honeycomb crystal after short relaxation at $t = 100$. (**c**,**d**) after the relaxation in the absence of noise at $t = 10{,}000$.

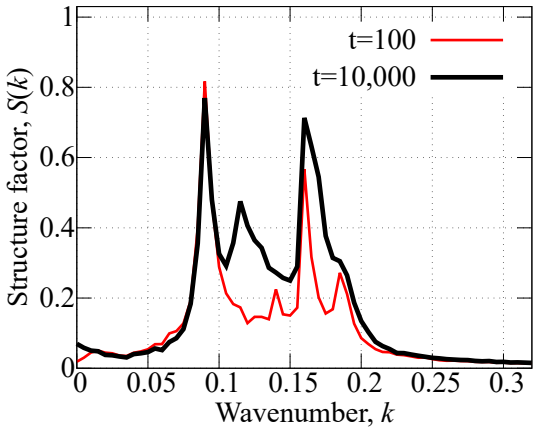

Figure 2. The normalized structure factor $S(k)$ was calculated for wavenumber k using the data obtained from the Fourier transform $\mathfrak{F}(n)$. The corresponding crystals can be found in Figure 1. Here, $t = 100$ corresponds to the initial n-distribution, and $t = 10,000$ represents the structural relaxation in the absence of noise.

Figure 2 shows the structure factor $S(k)$ as a function of the wave-number k for the ideal honeycomb after the short time $t = 100$ (see Figure 1a,b) and the slightly distorted crystal with blurred peaks of the atomic density n after the long relaxation $t = 10,000$; see Figure 1c,d. As shown by the black curve in Figure 2, the low-frequency (first) peak at $k \approx 0.08$ corresponds to the long-range order preserved during relaxation. The secondary

peaks at $k \approx 0.12$ and $k \approx 0.16$, also given by the black line in Figure 2, represent the appearance of two kinds of strain: (i) the shift in the maximum is associated with uniform strain; (ii) the blurring corresponds to the nonuniform strain and possible appearance of defects. We will use the position and width of the relaxed structure as a reference state for the study of defect induction.

4.2. Influence of the Uncorrelated Noise

The atomic density distribution n for the case of uncorrelated noise is presented in Figure 3. In this case, the last equation of Equation (8) is absent, and the noise term was set to the uncorrelated term $\vec{\zeta} = \vec{\xi}$. The long-wave contribution near $k = 0$ was analogous to the Rayleigh peak, which appeared when the hydrodynamic mode increased [12,42]. This peak degenerates with the high-frequency correlated fluctuations and growth of periodical structure modes. The significant blurring of the first split peak in Figure 3c is caused by the massive appearance of defects and degradation of the long-range order of the honeycomb crystal. The secondary peak (short-range order at $k \approx 0.17$) becomes broader due to the growth of the deformed honeycomb phase. The free energy of the system is not conserved, and a significant part of the domain volume is transferred to the quadratic phase, which can be associated with a shift in the melting curve [9] due to an increase in local density. As shown in Figure 3a, the honeycomb lattice experiences a significant number of defects and distortions, which can be interpreted in some cases as the appearance of a disordered phase (which is also observed from the wide first peak at $k \approx 0.11$ in Figure 3c) that is caused by a solid–solid transition. The sequence of the phases in the two-mode PFC model for a given q_0, q_1, r_0, and r_1 (see Table 1) is the triangle–honeycomb–square–striped phase [9]. Thus, due to the energy supplied by the delta-correlated white noise, we achieved the non-conservation of free energy. The details of these results were discussed in Refs. [12,43,44] in the form of hypotheses.

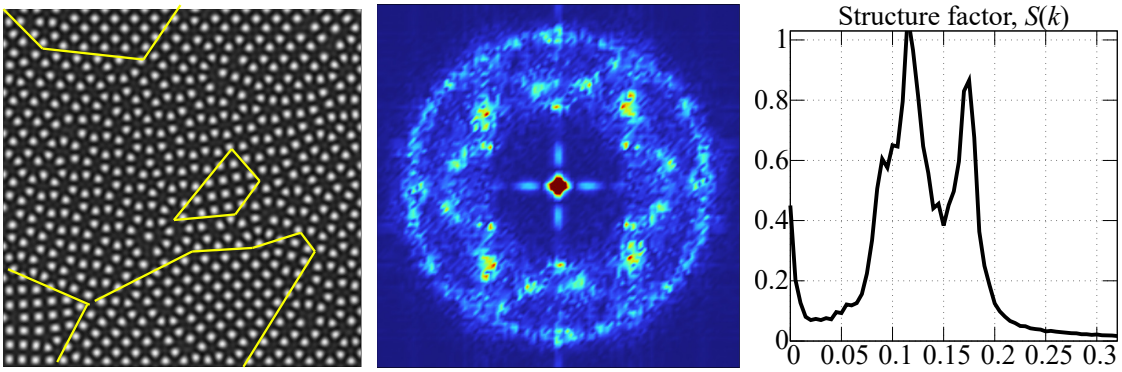

Figure 3. Uncorrelated noise at $t = 10{,}000$, noise amplitude $A = 1$, flux relaxation time $\tau = 0$. (**a**) Density distribution of n; the yellow lines correspond to the indicative grain boundaries. (**b**) Fourier transform $\mathfrak{F}(n)$. (**c**) Normalized structure factor $S(k)$, as function of wavenumber k.

4.3. Influence of the Parameters of Correlated Noise

The introduction of correlated noise by Equation (8) leads to the stabilization of the honeycomb structure for several values of the spatial noise correlation parameter λ_ζ; see Figures 4 and 5. One can observe the formation of two large grains in Figures 4a and 5a, but, in the first case where $\lambda_\zeta = 3$, one can find a more stable honeycomb structure. The bulk honeycomb structure is indicated by the peak corresponding to sixth-order symmetry in Figure 4b. The wide twin first peak in Figure 4c indicates the occurrence of the deformed honeycomb phase merging with the peak of the quadratic phase. One can find that deformed elongated honeycombs can generate a peak corresponding to the quasi-quadratic phase at $k \approx 0.11$, which can be clearly observed in Figure 5c. The broadening of the peaks represents multiple defects on the grain boundaries, in the domain around the

boundaries and in the case of vacancies with $\lambda_\zeta = 7$, as shown in Figure 5a. If significant statistics are gathered together with the Fourier analysis, one can quantitatively quantify the relative volume of defects and grain boundaries [45,46].

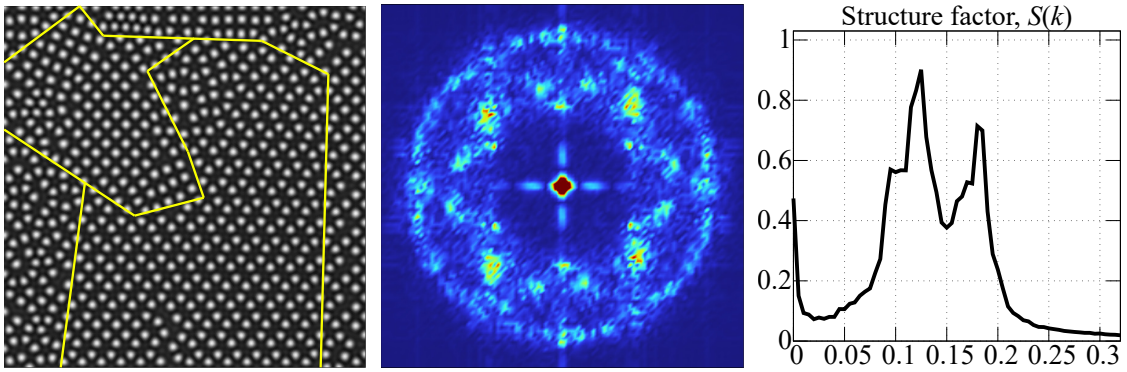

Figure 4. Stabilization of the honeycomb structure in the presence of correlated noise: $\lambda_\zeta = 3$, $\tau_\zeta = 1$, $\tau = 0$. (**a**) Density distribution of n; the yellow lines correspond to the indicative grain boundaries. (**b**) Fourier transform $\mathfrak{F}(n)$. (**c**) Normalized structure factor $S(k)$ as function of the wavenumber k.

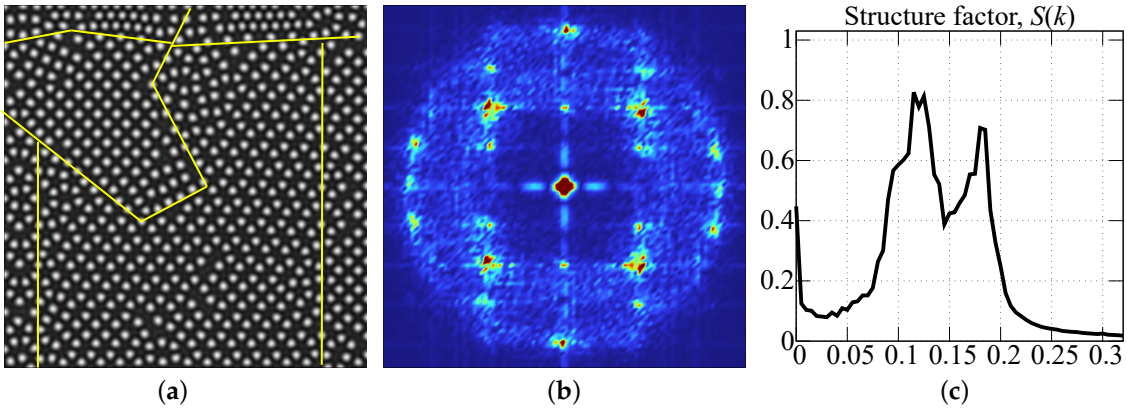

Figure 5. Appearance of bulk defects induced by correlated noise: $\lambda_\zeta = 7$, $\tau_\zeta = 1$, $\tau = 0$. (**a**) Density distribution of n; the yellow lines correspond to the indicative grain boundaries. (**b**) Fourier transform $\mathfrak{F}(n)$. (**c**) Normalized structure factor $S(k)$ as function of the wavenumber k.

As seen from the comparison of Figures 4 and 5, the gradual approach to the secondary lattice parameter $q \approx 6.7$ for the two-mode PFC leads to the accumulation of the noise-induced defects in the bulk. This contradicts the results of the formation of body-centered cubic crystals (BCC-crystals) for the single-mode PFC with amplification of the correlated noise [12], where $\lambda_\zeta \approx q$ leads to the effective stabilization of the periodic structure (here, q is the lattice parameter of the single-mode PFC model). However, in the present work, we investigated significantly larger grains and observed the formation of secondary phases in a very sensitive two-mode PFC model. As we observed in the computational results, the value $\lambda_\zeta = 7$ stabilizes mostly the quadratic phase.

The time correlation coefficient τ_ζ in the range of $1 \leq \tau_\zeta \leq 10$ has no essential influence on the formation of the defect structure of the honeycomb lattice. We assumed that the short temporal values of τ_ζ were caused by the fact that the characteristic time for defect migration and boundary motion was much longer than the noise–time correlation scale τ_ζ. In the physical sense, naturally, such times are comparable to the diffusion times $\tau_{diff} = \mathfrak{L}^2/\mathfrak{D}_0$, where $\mathfrak{L}$ is the characteristic length scale and $\mathfrak{D}_0$ is the diffusion coefficient (which, for our dimensionless case, is equal to the mobility coefficient M). For the slow correlations of $\tau_\zeta = 100$, one can observe, however, the grinding of the grains, intense destruction of the bulk crystal, and simultaneous formation of the quadratic phase, which can be

observed by the increasing peak of the quadratic phase in Figure 6a,d and corresponding broadening of structure factor in Figure 6b,c. Correlations in time fluctuations cause coherent vibrations on the diffusive time scale, which leads to increased mobility of the grain boundaries. The presence of the bright peak in Figure 6b at $\tau_\zeta = 1$–3 corresponds to the pseudo-quadratic phase linked with the stabilized honeycomb phase.

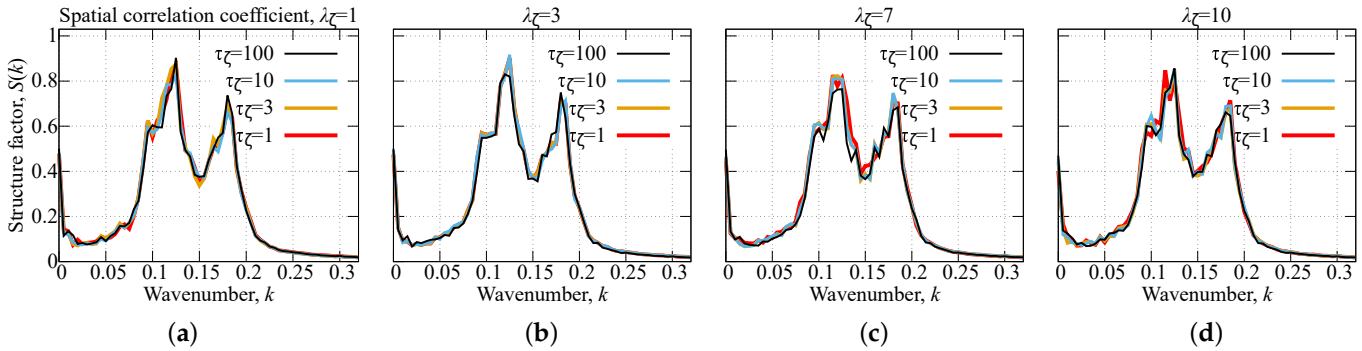

Figure 6. Normalized structure factors $S(k)$ were calculated for wavenumber k using the data obtained from Fourier transform $\mathfrak{F}(n)$ for different time correlation coefficients τ_ζ = 1–100 marked in color. Spatial-correlation coefficients: (**a**) $\lambda_\zeta = 1$; (**b**) $\lambda_\zeta = 3$; (**c**) $\lambda_\zeta = 7$; (**b**) $\lambda_\zeta = 10$.

Figure 7 shows the destruction of the bulk crystals and growth of the quadratic phase at $\tau_\zeta = 100$, which is also supported by the thermal-like influence of the short spatial correlation $\lambda_\zeta = 1$. The Fourier image and the structure factor $S(k)$ in Figure 7b,c show the presence of a distinct honeycomb and merged quadratic and quasi-quadratic phases. The broadening of the peaks occurred due to the disordered stripes of atomic density on the domain boundaries and the appearance of grain boundaries.

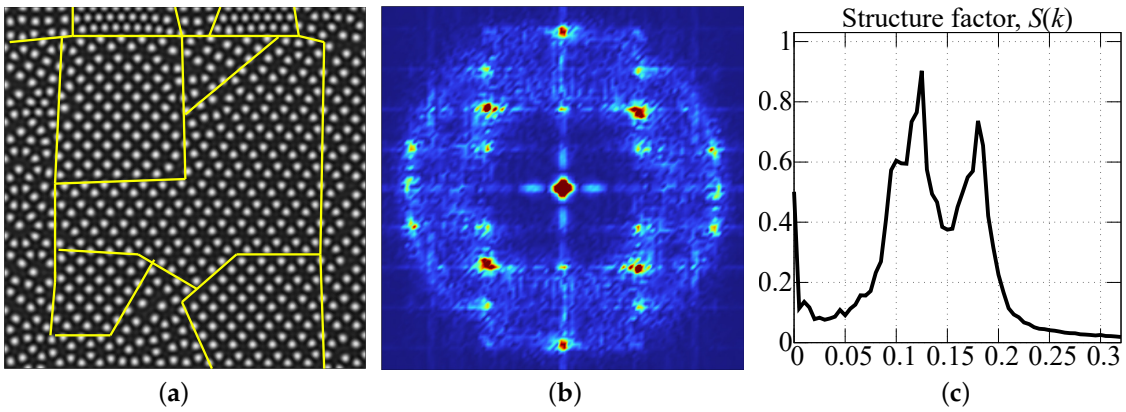

Figure 7. Destruction of the grains and massive appearance of the quadratic phase: $\lambda_\zeta = 1$, $\tau_\zeta = 100$, $\tau = 0$. (**a**) Density distribution of n; the yellow lines correspond to the indicative grain boundaries. (**b**) Fourier transform $\mathfrak{F}(n)$. (**c**) Normalized structure factor $S(k)$ as function of the wavenumber k.

The finite value of the atomic density flux relaxation, $\tau = 0.01$, leads to the limitation of the propagation of the velocity of disturbances, which causes substantial deceleration of the relaxation dynamics; see Figure 8. One can observe the formation of multiple grains with honeycomb, quadratic, and amorphous phases in Figure 8a, which is very similar to the defect patterns obtained in previous works [47,48]. Intensive destruction of the bulk of the ideal crystal occurs due to the inability of the computational domain to respond quickly to high-frequency spatio-temporal temperature fluctuations. Moreover, the increase in the value of the time correlation leads to collective fluctuations with lower frequency, which, for high τ_ζ and with the nonzero value of the relaxation time τ, leads to some grain coarsening. As a result of the computations, the disordered amorphous phases are clearly indicated in Figure 8b. The merging of low-density peaks can be observed in Figure 8c, which

demonstrates the mixing of the honeycomb and pseudo-quadratic phases. In conclusion, the finite nonzero value of the relaxation time τ for the atomic flux significantly slows the local relaxation of the fluctuating field and leads to grain fragmentation and the formation of disordered phases.

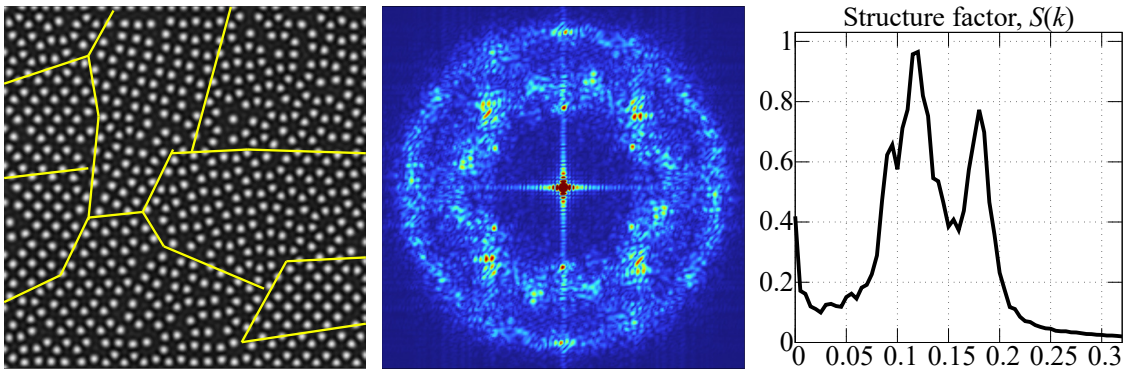

Figure 8. Grain refinement due to the finite value of flux relaxation time: $\lambda_\zeta = 1$, $\tau_\zeta = 1$, $\tau = 0.01$. (**a**) Density distribution of n; the yellow lines correspond to the indicative grain boundaries. (**b**) Fourier transform $\mathfrak{F}(n)$. (**c**) Normalized structure factor $S(k)$ as function of wavenumber k.

5. Conclusions

As one of the kinds of kinetic phase-field models, the modified phase-field crystal model (MPFC), described by the hyperbolic governing equation, has been used. The two-mode MPFC model has been advanced by the introduction of the correlated noise term. Periodic boundary conditions in the two-mode PFC model create the diffuse reflexes on the Fourier image of the atomic density after the relaxation of the initial honeycomb lattice. This effect occurs due to the presence of two lattice parameters in the two-mode approximation of the PFC equation. Indeed, the problem of the slight influence of the boundary conditions on the atomic density is absent in the single-mode approximation of the PFC equation with the only lattice parameter. With the introduction of white noise as an additive term in the governing PFC equation, the full energy of the computational domain is not conserved.

The time correlation coefficient τ_ζ in the colored noise:

- Acts as white (delta-correlated) noise at relatively small values of τ_ζ and within the short time intervals;
- Can lead to an increase in the boundary grain mobility and to the final refinement of the structure at a relatively large value of τ_ζ, comparable with the diffusion time.

The spatially correlated noise with the correlation coefficient λ_ζ leads to:

- The stabilization of the honeycomb structure at moderate values of the spatial noise correlation parameter $\lambda_\zeta \approx 3$;
- The observation of the origination of bulk defects at large values of $\lambda_\zeta \approx 10$.

The defects can be quantified and estimated using the free energy change in time for the entire computational domain. It would be enough to follow the evolution from an initially ideal lattice to a deformed/rotated/destroyed lattice with the calculation of the free energy. Such methodology may be developed in a future work.

One of the key perspectives in the development of the present work is also seen in the reproduction of the cooled noise adequately to the experimental/computation influence of the transformation in the sample under study. The finding of the ranges of colored noise parameters, which can imitate external processing and be consistent with the influence of an external field (such as irradiation) or internal processes (such as corrosion), seems to be a natural advancement of the present methodology.

Author Contributions: P.K.G. and V.A. contributed equally to the design of this study, the implementation of the research, the analysis of the results, and the writing of the manuscript. All authors have read and agreed to the published version of the manuscript.

Funding: This study was financially supported by the Russian Science Foundation, project 19-79-20012.

Data Availability Statement: The data presented in this study are available in the article.

Acknowledgments: The authors thank Evgeny Kharanzhevskiy for fruitful discussions and encouragement of this work.

Conflicts of Interest: The authors declare no conflict of interest.

References

1. Crawford, J.H.; Slifkin, L.M. (Eds.) *Point Defects in Solids*; Springer: Boston, MA, USA, 1972; p. 556. [CrossRef]
2. Ashkenazy, Y.; Averback, R.S. Irradiation induced grain boundary Flow—A new creep mechanism at the nanoscale. *Nano Lett.* **2012**, *12*, 4084–4089. [CrossRef] [PubMed]
3. Hirvonen, P.; Heinonen, V.; Dong, H.; Fan, Z.; Elder, K.R.; Ala-Nissila, T. Phase-field crystal model for heterostructures. *Phys. Rev. B* **2019**, *100*, 165412. [CrossRef]
4. Shuai, X.; Mao, H.; Kong, Y.; Du, Y. Phase field crystal simulation of the structure evolution between the hexagonal and square phases at elevated pressures. *J. Min. Metall. Sect. B Metall.* **2017**, *53*, 271–278. [CrossRef]
5. Gao, N.; Zhao, Y.; Xia, W.; Liu, Z.; Lu, X. Phase-Field Crystal Studies on Grain Boundary Migration, Dislocation Behaviors, and Topological Transition under Tension of Square Polycrystals. *Crystals* **2023**, *13*, 777. [CrossRef]
6. Zhang, F.; Li, D.; Sun, H.W. Efficient and energy stable numerical schemes for the two-mode phase field crystal equation. *J. Comput. Appl. Math.* **2023**, *427*, 115148. [CrossRef]
7. Ankudinov, V.; Galenko, P.K. Structure diagram and dynamics of formation of hexagonal boron nitride in phase-field crystal model. *Philos. Trans. Ser. A Math. Phys. Eng. Sci.* **2022**, *380*, 20200318. [CrossRef] [PubMed]
8. Ankudinov, V.; Galenko, P. Growth of two-dimensional hexagonal lattices in phase-field crystal model. *JETP Lett.* **2022**, *115*, 778–785. [CrossRef]
9. Ankudinov, V.E. Formation and Stability of the Crystalline Structures in Two-Mode Phase-Field Crystal Model. *Phys. Solid State* **2022**, *64*, 417–424. [CrossRef]
10. Kharchenko, V.O.; Kharchenko, D.O. Noise-induced pattern formation in system of point defects subjected to irradiation. *Eur. Phys. J. B* **2012**, *85*, 383. [CrossRef]
11. Kharchenko, D.O.; Kharchenko, V.O.; Bashtova, A.I. Modeling self-organization of nano-size vacancy clusters in stochastic systems subjected to irradiation. *Radiat. Eff. Defects Solids* **2014**, *169*, 418–436. [CrossRef]
12. Ankudinov, V.; Starodumov, I.; Kryuchkov, N.P.; Yakovlev, E.V.; Yurchenko, S.O.; Galenko, P.K. Correlated noise effect on the structure formation in the phase-field crystal model. *Math. Methods Appl. Sci.* **2021**, *44*, 12185–12193. [CrossRef]
13. Galenko, P.K. *Phase Field Theory in Materials Physics: The Hodograph Equation*; Springer: Berlin/Heidelberg, Germany, 2024.
14. Galenko, P.; Jou, D. Diffuse-interface model for rapid phase transformations in nonequilibrium systems. *Phys. Rev. E* **2005**, *71*, 046125. [CrossRef] [PubMed]
15. Galenko, P.; Danilov, D.; Lebedev, V. Phase-field-crystal and Swift-Hohenberg equations with fast dynamics. *Phys. Rev. E* **2009**, *79*, 51110. [CrossRef] [PubMed]
16. Conti, M.; Giorgini, A.; Grasselli, M. Phase-field crystal equation with memory. *J. Math. Anal. Appl.* **2016**, *436*, 1297–1331. [CrossRef]
17. Wang, C.; Wise, S. An energy stable and convergent finite difference scheme for the modified phase field crystal equation. *SIAM J. Numer. Anal.* **2011**, *49*, 945–969. [CrossRef]
18. Wang, C.; Wise, S. Global smooth solutions of the three dimensional modified phase field crystal equation. *Methods Appl. Anal.* **2010**, *17*, 191–212. [CrossRef]
19. Stefanovic, P.; Haataja, M.; Provatas, N. Phase-field crystals with elastic interactions. *Phys. Rev. Lett.* **2006**, *96*, 225504. [CrossRef] [PubMed]
20. Stefanovic, P.; Haataja, M.; Provatas, N. Phase field crystal study of deformation and plasticity in nanocrystalline materials. *Phys. Rev. E* **2009**, *80*, 046107. [CrossRef]
21. Archer, A.J. Dynamical density functional theory for molecular and colloidal fluids: A microscopic approach to fluid mechanics. *J. Chem. Phys.* **2009**, *130*, 014509. [CrossRef]
22. Lebedev, V.; Sysoeva, A.; Galenko, P. Unconditionally gradient-stable computational schemes in problems of fast phase transitions. *Phys. Rev. E* **2011**, *83*, 026705. [CrossRef]
23. Galenko, P.K.; Gomez, H.; Kropotin, N.V.; Elder, K.R. Unconditionally stable method and numerical solution of the hyperbolic phase-field crystal equation. *Phys. Rev. E* **2013**, *88*, 13310. [CrossRef] [PubMed]
24. García-Ojalvo, J.; Sancho, J.M. Colored noise in spatially extended systems. *Phys. Rev. E* **1994**, *49*, 2769–2778. [CrossRef] [PubMed]
25. Galenko, P.K.; Kharchenko, D.; Lysenko, I. Stochastic generalization for a hyperbolic model of spinodal decomposition. *Phys. A Stat. Mech. Its Appl.* **2010**, *389*, 3443–3455. [CrossRef]

26. Wu, K.A.K.A.; Karma, A. Phase-field crystal modeling of equilibrium bcc-liquid interfaces. *Phys. Rev. B* **2007**, *76*, 184107. [CrossRef]
27. Jaatinen, A.; Achim, C.V.; Elder, K.R.; Ala, T. Thermodynamics of bcc metals in phase-field-crystal models. *Phys. Rev. E* **2009**, *80*, 031602. [CrossRef] [PubMed]
28. Elder, K.R.; Huang, Z.F.; Provatas, N. Amplitude expansion of the binary phase-field-crystal model. *Phys. Rev. E* **2010**, *81*, 011602. [CrossRef] [PubMed]
29. Huang, Z.F.; Elder, K.R.; Provatas, N. Phase-field-crystal dynamics for binary systems: Derivation from dynamical density functional theory, amplitude equation formalism, and applications to alloy heterostructures. *Phys. Rev. E* **2010**, *82*, 021605. [CrossRef]
30. V.V.Lebedev, A. Theory of weak crystallization of films. *Sov. Phys. Solid State* **1990**, *32*, 493–495.
31. Kats, E.I.; Lebedev, V.V.; Muratov, A.R. Weak crystallization theory. *Phys. Rep.* **1993**, *228*, 1–91. [CrossRef]
32. Wu, K.A.; Adland, A.; Karma, A. Phase-field-crystal model for fcc ordering. *Phys. Rev. E* **2010**, *81*, 61601. [CrossRef]
33. Lifshitz, R.; Petrich, D.M. Theoretical model for faraday waves with multiple-frequency forcing. *Phys. Rev. Lett.* **1997**, *79*, 1261–1264. [CrossRef]
34. Ankudinov, V.; Elder, K.R.; Galenko, P.K. Traveling waves of the solidification and melting of cubic crystal lattices. *Phys. Rev. E* **2020**, *102*, 062802. [CrossRef] [PubMed]
35. Emdadi, A.; Asle Zaeem, M.; Asadi, E. Revisiting phase diagrams of two-mode phase-field crystal models. *Comput. Mater. Sci.* **2016**, *123*, 139–147. [CrossRef]
36. Ryzhov, V.N.; Tareyeva, E.E. Towards a statistical theory of freezing. *Phys. Lett. A* **1979**, *75*, 88–90. [CrossRef]
37. Ramakrishnan, T.V.; Yussouff, M. First-principles order-parameter theory of freezing. *Phys. Rev. B* **1979**, *19*, 2775–2794. [CrossRef]
38. Tóth, G.I.; Tegze, G.; Pusztai, T.; Tóth, G.; Gránásy, L. Polymorphism, crystal nucleation and growth in the phase-field crystal model in 2D and 3D. *J. Phys. Condens. Matter* **2010**, *22*, 364101. [CrossRef]
39. *COMSOL Multiphysics® v. 6.0*; COMSOL AB: Stockholm, Sweden, 2022. Available online: www.comsol.com (accessed on 12 December 2023).
40. Ankudinov, V.; Galenko, P.K. Growth of different faces in a body centered cubic lattice: A case of the phase-field-crystal modeling. *J. Cryst. Growth* **2020**, *539*, 125608. [CrossRef]
41. Mkhonta, S.K.; Elder, K.R.; Huang, Z.F. Exploring the complex world of two-dimensional ordering with three modes. *Phys. Rev. Lett.* **2013**, *111*, 35501. [CrossRef]
42. Hansen, J.P.; McDonald, I.R. *Theory of Simple Liquids*, 3rd ed.; Elsevier Academic Press: Amsterdam, The Netherlands, 2006; pp. 1–416. [CrossRef]
43. Marconi, U.M.B.; Tarazona, P. Dynamic density functional theory of fluids. *J. Chem. Phys.* **1999**, *110*, 8032–8044. [CrossRef]
44. Van Teeffelen, S.; Backofen, R.; Voigt, A.; Löwen, H. Derivation of the phase-field-crystal model for colloidal solidification. *Phys. Rev. E-Stat. Nonlin. Soft Matter Phys.* **2009**, *79*, 051404. [CrossRef]
45. Delhez, R.; de Keijser, T.; Mittemeijer, E.; Langford, J. Size and Strain Parameters from Peak Profiles: Sense and Nonsense. *Aust. J. Phys.* **1988**, *41*, 213. [CrossRef]
46. Snyder, R.L.; Fiala, J.; Bunge, H.J. *Defect and Microstructure Analysis by Diffraction*; Oxford University Press: Oxford, UK, 2000; p. 808. [CrossRef]
47. Zhang, W.; Mi, J. Phase field crystal modelling of the order-to-disordered atomistic structure transition of metallic glasses. *IOP Conf. Ser. Mater. Sci. Eng.* **2016**, *117*, 012056. [CrossRef]
48. Berry, J.; Grant, M. Phase-field-crystal modeling of glass-forming liquids: Spanning time scales during vitrification, aging, and deformation. *Phys. Rev. E-Stat. Nonlin. Soft Matter Phys.* **2014**, *89*, 062303. [CrossRef] [PubMed]